PAPER

Attosecond transient absorption of a bound wave packet coupled to a smooth continuum

IOP Publishing Journal of Optics
J. Opt. **19** (2017) 114004 (9pp) https://doi.org/10.1088/2040-8986/aa8a93

Attosecond transient absorption of a bound wave packet coupled to a smooth continuum

Jan Marcus Dahlström[1,2], **Stefan Pabst**[3,4] and **Eva Lindroth**[2]

[1] Department of Physics, Lund University, Box 118, SE-221 00 Lund, Sweden
[2] Department of Physics, Stockholm University, AlbaNova University Center, SE-106 91 Stockholm, Sweden
[3] ITAMP, Harvard-Smithsonian Center for Astrophysics, 60 Garden Street, Cambridge, MA 02138, United States of America
[4] Stanford PULSE Institute, SLAC National Accelerator Laboratory, Menlo Park, CA 94025, United States of America

E-mail: marcus.dahlstrom@matfys.lth.se

Received 29 June 2017, revised 27 August 2017
Accepted for publication 6 September 2017
Published 16 October 2017

Abstract

We investigate the possibility of using transient absorption of a coherent bound electron wave packet in hydrogen as an attosecond pulse characterization technique. In a recent work, we have shown that photoionization of such a coherent bound electron wave packet opens up for pulse characterization with unprecedented temporal accuracy—independent of the atomic structure—with maximal photoemission at all kinetic energies given a wave packet with zero relative phase (Pabst and Dahlström *Phys. Rev.* A **94** 13411 (2016)). Here, we perform numerical propagation of the time-dependent Schrödinger equation and analytical calculations based on perturbation theory to show that the energy-resolved maximal absorption of photons from the attosecond pulse does *not* uniquely occur at a zero relative phase of the initial wave packet. Instead, maximal absorption occurs at different relative wave packet phases, distributed as a non-monotonous function with a smooth $-\pi/2$ shift across the central photon energy (given a Fourier-limited Gaussian pulse). Similar results are also found in helium. Our finding is surprising, because it implies that the energy-resolved photoelectrons are not mapped one-to-one with the energy-resolved absorbed photons of the attosecond pulse.

Keywords: attosecond, transient absorption, ATAS, pulse characterization, continuum transition

(Some figures may appear in colour only in the online journal)

1. Introduction

Ultra-short optical laser pulses provide the required time-resolution for femtochemistry: the study of molecular motion and transition states [1], but optical pulses can not be made short enough to probe the valence electron motion in atoms and molecules, which typically occur on the attosecond or few femtosecond time scale. Today, it is possible to reach the electron time scale using attosecond pulses of coherent extreme ultraviolet (XUV) or x-ray radiation, which has opened up for attophysics the study of electron motion in atoms and molecules [2]. As attophysics is the natural continuation of femtochemisty, it is not surprising that many experimental ideas have already been transfered from the femtosecond to the attosecond domain. One example of such a technique is attosecond transient absorption spectroscopy (ATAS), which has been used to study electron coherences and to reconstruct the motion of valence electrons in atoms [3–5]. With increasing photon energies, time-resolved x-ray absorption spectroscopy (TR-XAS) makes it possible to follow element-specific dissociation of molecules in real time [6]. In the above mentioned experiments, an intense laser field was used to prepare a wave packet in the target system, while the coherent XUV/x-ray light was used as a probe of the dynamics. The reverse scenario is also possible, where, instead, the attosecond pulse is used to trigger electron dynamics that are sequentially probed with the strong laser field that couples populated autoionizing states to dark states.

This gives rise to numerous effects, including control of the Fano line shape, light-induced states and Autler-Townes splitting [7–9], and to the observation of counter-rotating wave effects [10]. An overview of the experimental work with ATAS is given in [11].

The ATAS method has been studied extensively in theory with the main focus on the description of dynamics of laser-coupled autoionizing states [12] and on the pulse overlap (non-sequential) region [13]. The theory of strong-field ATAS is comprehensively reviewed in [14], but the simple case of ATAS sequentially coupled to a smooth (resonance free) continuum by an attosecond pulse has not yet been considered. The question arises if autoionizing states are required to control absorption of the attosecond pulse or if it is possible to exert similar control when ATAS is coupled to a smooth continuum.

In light of our recent proposal, where we showed that sequential photoionization of a bound wave packet can be used as a characterization method for attosecond pulses with unprecedented temporal accuracy [15, 16], we ask the question: can ATAS serve as an all-optical pulse characterization method? The article is organized as follows. We outline the theory of our method in section 2 and give details about the numerical propagation scheme in section 3 and about the analytical calculations in section 4. In section 5, we present our main results and, in section 6, we present our conclusions.

2. Theory

We write the time-dependent Schrödinger equation (TDSE) for a single electron as

$$i|\dot{\psi}(t)\rangle = \hat{H}(t)|\psi(t)\rangle = [\hat{H}_0 + \hat{V}_I(t)]|\psi(t)\rangle, \tag{1}$$

where the total Hamiltonian, $\hat{H}$, consists of a time-independent atomic operator, $\hat{H}_0$, and a time-dependent field-interaction operator,

$$\hat{V}_I(t) = A(t)\hat{p}_z + \frac{1}{2}A^2(t). \tag{2}$$

The field-interaction in this form assumes a linearly polarized vector potential, $A(t)$, along the z-axis within the velocity gauge dipole approximation with the z-component of the momentum operator denoted as $\hat{p}_z$. The eigenstates of the atomic Hamiltonian are denoted by $|j\rangle$ with eigenvalues, ϵ_j. We use short-hand notation $|j\rangle$ to label all states with atomic quantum numbers for bound states (n_j, ℓ_j, m_j) and energy-normalized continuum states $(\epsilon_j, \ell_j, m_j)$. Atomic units are used unless otherwise stated, $e = \hbar = m_e = 4\pi\epsilon_0 = 1$.

2.1. Gauge consideration

In the following, we will refer to the vector potential in equation (2) as the *test pulse*. It is common practice to remove the interaction term proportional to $A^2(t)$. This omission can be fully justified [17], also in cases when the test pulse is strong, by performing a spatially uniform, time-dependent gauge transformation, $|\psi\rangle = \exp(i\Lambda)|\tilde{\psi}\rangle$, where

$$\Lambda(t) = -\int^t dt' \frac{1}{2}A^2(t'). \tag{3}$$

While this unitary transformation leaves the expectation value of the canonical momentum operator unchanged,

$$p_z(t) = \langle\psi \mid \hat{p}_z|\psi\rangle = \langle\tilde{\psi} \mid \hat{p}_z \mid \tilde{\psi}\rangle, \tag{4}$$

it does involve a subtle re-definition of the absolute energy scale at each moment in time that we need to be aware of in the following work. Finally, we add that the expectation value of the position operator in length gauge (L) is identical to that computed using the wave functions from velocity gauge (V),

$$z(t) = \langle\psi^{(L)} |\hat{z} \mid \psi^{(L)}\rangle = \langle\psi^{(V)} \mid \hat{z} \mid\psi^{(V)}\rangle, \tag{5}$$

which can be shown with the associated well-known gauge transformation,

$$\Lambda'(z, t) = -zA(t). \tag{6}$$

2.2. Initial bound wave packet and model test pulse

We will consider that the initial condition for the TDSE in equation (1) is a field-free wave packet consisting of N bound states labeled by j,

$$|\psi^{(0)}(t)\rangle = \sum_j^N c_j(t)\exp[-i\epsilon_j t]|j\rangle, \tag{7}$$

where $c_j(t)$ are complex amplitudes that are constant under free-field conditions (before the test pulse arrives on target). The scheme for preparing the wave packet is not important, but it is essential that it is sequential. This means that the preparation of the wave packet is finished before the test pulse arrives at the atom. It goes without saying that the wave packet is assumed to be fully coherent with the test pulse.

As mentioned in the introduction, the role of excitation to (quasi) bound states has been studied recently by isolated attosecond pulses. In this paper, we study the case where the test pulse ionizes the atom, i.e. the central frequency is larger than the ionization potential: $\omega_0 > I_p$, with excitation to a smooth continuum of states. As a concrete example, we will consider the following two-state wave packet and test pulse:

$$\text{Wave packet}: \begin{cases} c_1 & = c_2 & = 1/\sqrt{2} \\ \epsilon_{j_1} & = 0.375 & = 10.20\ \text{eV} \\ \epsilon_{j_2} & = 0.444 & = 12.09\ \text{eV} \\ I_p & = 0.5 & = 13.61\ \text{eV} \end{cases}$$

$$\text{Test pulse}: \begin{cases} \omega_0 & = 1.5 & = 40.81\ \text{eV} \\ \tau_e & = 5.0 & = 120.94\ \text{as}, \end{cases} \tag{8}$$

where the atomic energies correspond to a $2s/3s$-wave packet in the hydrogen atom. The vector potential is modeled by an oscillating Gaussian pulse,

$$A(t) = A_0\cos[\omega_0(t - t_0) + \phi]\exp[-a(t - t_0)^2], \tag{9}$$

where A_0 is the envelope amplitude, τ_0 is the arrival time of the envelope, ϕ is the carrier-envelope phase (CEP) and $a = 2\ln(2)/\tau_e^2$ is inversely proportional to the squared envelope duration, τ_e, expressed in full-width at half-maximum (FWHM).

2.3. Energy absorbed by atom

Due to total energy conservation, it is possible to infer the absorbed energy from the test pulse by instead calculating the energy gained by the excited atom, $\Delta\mathcal{E}$. This latter quantity can be formally expressed as [14]

$$\Delta\mathcal{E} = \int_{-\infty}^{+\infty} \mathrm{d}t \frac{\mathrm{d}\Delta\mathcal{E}}{\mathrm{d}t}, \tag{10}$$

where $\Delta\mathcal{E}(t)$ is the time-dependent expectation value of the atomic energy in the field. The instantaneous power delivered to the atom in velocity gauge becomes

$$\begin{aligned}\frac{\mathrm{d}\Delta\mathcal{E}}{\mathrm{d}t} &= \frac{\mathrm{d}}{\mathrm{d}t}\langle\psi(t) \mid \hat{H}(t) \mid \psi(t)\rangle \\ &= [p_z(t) + A(t)]\dot{A}(t) = -\Pi_z(t)E(t),\end{aligned} \tag{11}$$

which is gauge invariant, because it involves the kinetic momentum, $\Pi_z = p_z + A$, and the electric field, $E = -\dot{A}$. Equation (11) is analogous to the expression found in classical electrodynamics when computing the power transfered to a classical system. If, instead, we were to use the gauge transformed Hamiltonian (without the $\frac{1}{2}A^2(t)$ term) then the $A\dot{A}$ term in equation (11) would be missing and it would be the canonical momentum that is multiplied with the electric field. Clearly, this power is not gauge invariant then, because it must be related to the time-dependent absolute energy associated with the unitary transformation in equation (3), but the total energy gain is gauge invariant because

$$\int_{-\infty}^{+\infty} \mathrm{d}t A(t)\dot{A}(t) = \left[\frac{1}{2}A^2(t)\right]\Bigg|_{-\infty}^{+\infty} = 0, \tag{12}$$

provided that the test pulse is finite in time. The $A\dot{A}$ term is universal because it does not involve any reference to the specific atomic system under investigation. Instead, it can be interpreted as the power delivered to a free electron with no initial or final momentum, but with a field-induced momentum, $A(t)$, during the action of the test pulse. In this interpretation, it is clear that the integrated power (total energy gain) mediated by the $A\dot{A}$ term must vanish as a free electron should be unable to gain energy from any given test pulse.

Following [14], but instead using a velocity gauge, the total energy gain in equation (10) can be rewritten in the energy domain as

$$\Delta\mathcal{E} = -2\int_0^{+\infty} \mathrm{d}\omega\, \omega\, \mathrm{Im}\{[\tilde{p}_z(\omega) + \tilde{A}(\omega)]\tilde{A}^*(\omega)\}, \tag{13}$$

where $\tilde{p}_z(\omega) = \tilde{p}_z^*(-\omega)$ and $\tilde{A}(\omega) = \tilde{A}^*(-\omega)$ are the Fourier transforms of the real $p_z(t)$ and $A(t)$ functions, respectively. This implies that the energy-resolved absorbed energy from the test pulse (or gained by the atom) is

$$\frac{\mathrm{d}\Delta\mathcal{E}}{\mathrm{d}\omega} = -2\omega\, \mathrm{Im}\{\tilde{p}_z(\omega)\tilde{A}^*(\omega)\}, \tag{14}$$

where we have used the fact that the term $\tilde{A}\tilde{A}^* = |\tilde{A}|^2$ in equation (13) is real. We find that the $A\dot{A}$ term in equation (11) does not contribute to absorption of the test pulse at *any* energy. In other words, the energy density in equation (14) is invariant with respect to the unitary transformation given by equation (3), in contrast to the power given in equation (11).

3. Numerical propagation

In this section, we discuss our numerical approach to study the absorption of a test pulse by a coherent wave packet in hydrogen and noble gas atoms, such as helium. The effective radial Schrödinger equation is

$$\left[-\frac{1}{2}\frac{\partial^2}{\partial r^2} + \frac{1}{2}\frac{\ell(\ell+1)}{r^2} - \frac{Z}{r} + u_{\mathrm{HF}}\right]\psi_j(r) = \epsilon_j\psi_j(r), \tag{15}$$

where Z is the nuclear charge and u_{HF} is the Hartree–Fock potential (for hydrogen we have $Z = 1$ and $u_{\mathrm{HF}} = 0$). We use a primitive basis set of B-splines [18] to find the diagonalized hydrogen states, or restricted Hartree–Fock (HF) orbitals [19], using codes developed earlier in Stockholm for time-independent calculations; see [20–22]. The eigenstates are labeled by j for a given electron state and expressed in non-orthogonal B-splines labeled by n,

$$\psi_j(r) = \sum_n^{N_b} b_n^{(j)} B_n(r), \tag{16}$$

with complex amplitudes $b_n^{(j)}$. We use B-splines of order $k = 5$ with a grid of $N_p = 220$ knot points, thus, generating a total number of $N_b = N_p - k - 2 = 213$ B-splines that vanish at the radial boundaries of the grid. The knot points are placed in the complex plane in accordance with exterior complex scaling (ECS) [23],

$$r \to \begin{cases} r, & 0 < r < R_C \\ R_C + (r - R_C)\mathrm{e}^{\mathrm{i}\theta}, & r > R_C \end{cases}, \tag{17}$$

where the radial coordinate is transformed beyond a radius $R_C = 75$ with a complex angle of $\theta = 15°$. A wave packet expressed as a superposition of eigenstates of the scaled Hamiltonian is physical in the inner region, $r < R_C$, while it is exponentially damped (unphysical) in the outer region, $r > R_C$. We place 17 knot points in this outer region to account for the damping from 75 to 90 along the real axis. ECS is a useful tool for numerical propagation as it avoids numerical reflections at the end of the numerical box, see [24], where the complex scaling is done all the way to infinity.

The TDSE is propagated on the HF basis similar to the time-dependent configuration-interaction singles (TDCIS) implementation presented in [13, 25], but here we are restricted to propagation in the velocity gauge (V), due to ECS [26]. Nonetheless, it is possible to also compute the time-dependent dipole in the length gauge (L) using the 'physical' (V)-wave packet in the inner region, as discussed in connection with equation (5). In practice, this is done easily by truncating the summation of B-splines (equation (16)) when constructing the operators so that only unscaled (real) B-splines are used to compute the radial part of the dipole matrix elements. We have verified that changing the position

of the truncation does not alter the results presented in this paper.

3.1. Hydrogen: 2s/3s wave packet

We now consider the initial $2s/3s$ wave packet in hydrogen and pulse parameters shown in equations (8)–(9) with a weak field strength $A_0 = 0.01$. In figure 1(a), we show the corresponding time-dependent expectation values of position and kinetic momentum of the electron. The electron oscillates during the test pulse, see $z(t)$, with a phase lag of $\sim\pi$ relative the driving force of the test pulse, $-E(t)$. In analogy with a damped simple harmonic oscillator, this π-shift implies a strongly over-driven system, i.e. the electron has a hard time keeping up with the fast oscillations of the test pulse. The kinetic momentum, $\Pi_z(t)$, is shifted by $\sim\pi/2$ in between force and position, as expected for an oscillating system. The expectation values oscillate only during the overlap region with the test pulse. The expectation values of an unprepared hydrogen atom (in the $1s$ state) look qualitatively the same (not shown).

In figure 1(b), we show the instantaneous power delivered to the atom according to equation (11) in the velocity gauge, both with and without the $\frac{1}{2}A^2$ term, as well as the length-gauge expression used by Wu *et al* in [14],

$$\Delta\dot{\mathcal{E}}^{(L)}(t) = z(t)\dot{E}(t). \tag{18}$$

The power delivered to the atom during the action of the test pulse is gauge dependent. In the length gauge and the transformed velocity gauge (without $\frac{1}{2}A^2(t)$), the power oscillates between positive and negative values, which implies that the power is delivered and extracted at a fast rate during the test pulse. At the center of the test pulse, the power oscillations are π-shifted with respect to length and transformed velocity gauge, which shows that the interpretation of these quantities as 'power' is debatable. In the velocity gauge, the power looks dramatically different: it is purely positive and much smaller in magnitude. It is known from text books on quantum mechanics, see [27], that the absolute energy scale is shifted by a spatially uniform time-dependent gauge transform, such as $\frac{1}{2}A^2(t)$. This explains the difference between the transformed and original velocity gauge power, because the time-dependent redefinition of the absolute energy scale can be taken into account by adding $-A(t)E(t)$ to the transformed velocity gauge result, giving back the velocity result. From these considerations, we consider the velocity gauge as the correct 'physical' convention for the instantaneous power.

In figure 1(c), we show the energy gain (integrated power) delivered to the atom as a function of time. Again, during the action of the test pulse, the energy gain is gauge dependent. The length gauge and the transformed velocity gauge show large oscillations of the energy gain, while the physical energy delivered (velocity gauge) shows that the energy is gradually increased in small steps toward the final value. After the test pulse is over, however, the total energy gain is identical in all three gauges, which shows that either gauge can be used to compute the total energy gained by the test pulse.

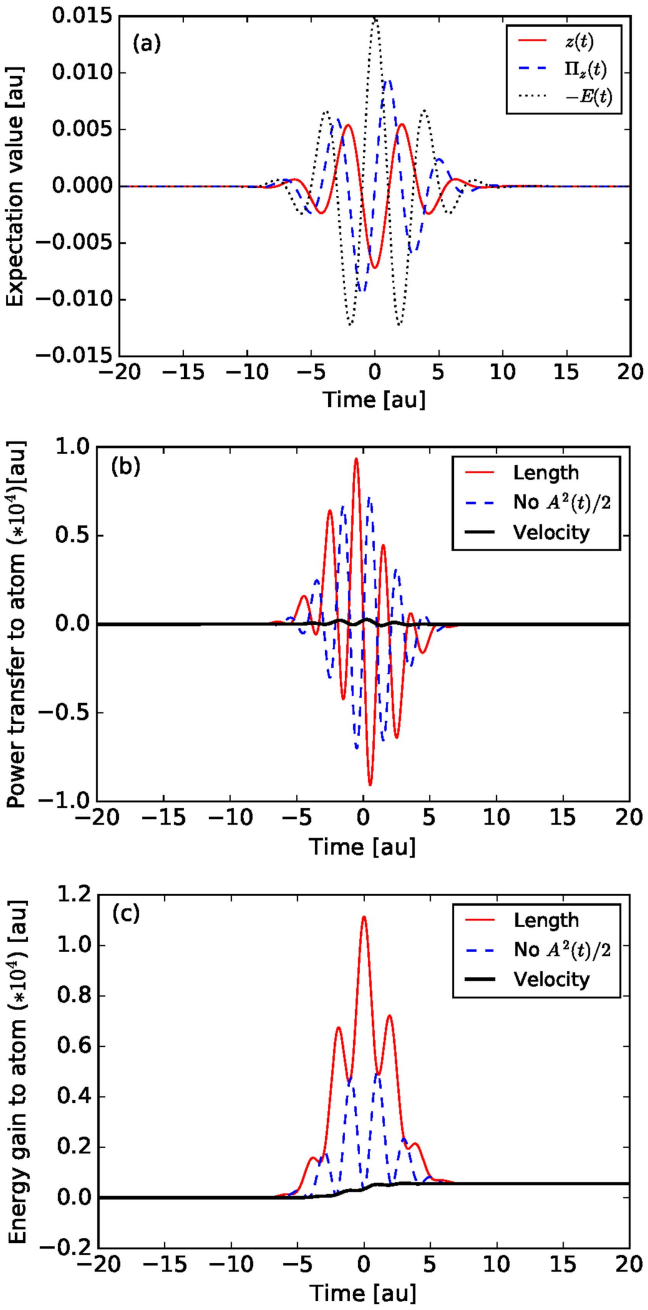

Figure 1. (a) Time-dependent expectation values of position and kinetic momentum induced by test pulse starting with a $2s/3s$ hydrogen wave packet. The force (minus electric field) of the test pulse is plotted for direct comparison. (b) Power delivered to the atom as a function of time. (c) Energy delivered to the atom as a function of time. See the main text for details about the three different gauges.

In figure 2, we show the energy absorbed by the 2s/3s wave packet in the hydrogen atom resolved in photon energy, evaluated by equation (14). The normalized Fourier transform of the electric field and vector potential are shown for comparison. The peak of absorption is located close to the central photon frequency, $\omega_0 = 1.5$, in good agreement with the peak of the vector potential, while the electric field peak is located at a slightly higher energy. Finally, we note that the energy

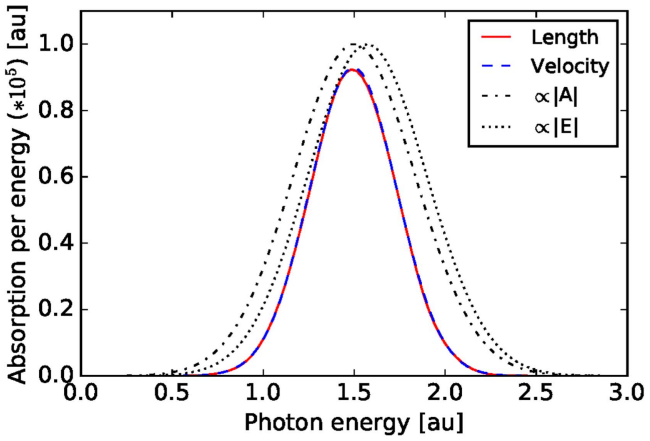

Figure 2. Energy absorbed by the hydrogen atom, initially in a 2s/3s wave packet, resolved over photon energies. The normalized electric field and vector potential are shown for comparison in the energy domain. The data has been interpolated between discrete values by a cubic spline function.

Table 1. Absorbed energy by the hydrogen atom prepared in different initial states before the arrival of the test pulse.

Initial state:	Absorption [au]:
1*s*	6.87e-05
2*s*	7.38e-06
3*s*	2.14e-06

resolved absorption is gauge invariant for the hydrogen wave packet.

In table 1, we show the total absorption of energy from the first three *s*-wave states in hydrogen individually. The absorption is decreasing with increasing principal quantum number and the ratio of 2s/3s is 3.45.

The question then arises as to how a delay of the coherent 2s/3s wave packet can change the absorption of the test pulse. In order to study this effect, we assume that

$$c_2 = c_1 \exp[i\varphi] \tag{19}$$

where φ is the relative phase of the initial wave packet (not the CEP phase of the test pulse defined in equation (9)). In figure 3, we show the energy-resolved absorption as a function of φ in false color. The absorption of energy from the test pulse is most efficient if the wave packet states are in phase with each other, $\varphi \approx 0$. Conversely, if the wave packet states have opposite phases, $\varphi \approx \pi$, then the absorption is reduced. The atom can not be made completely transparent for the test pulse, but the energy gain can be dramatically reduced by almost an order of magnitude. Further, there is a tilt in the absorption map, where the low (high) photon energies require a slightly larger (smaller) relative phase to maximize the absorption. This observation is surprising, given our recent work on pulse characterization using *photoemission* from coherent bound wave packets, referred to as pulse analysis by delayed absorption (PANDA) [15, 16]. When using the

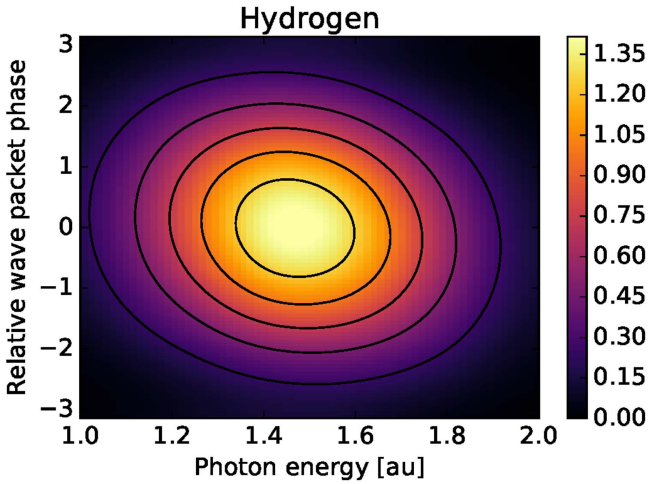

Figure 3. The absorbed energy ($*10^5$) from the test pulse by the $2s/3s$ hydrogen wave packet as a function of photon energy and relative wave packet phase, φ. The data has been interpolated between discrete values by a cubic spline function.

PANDA method, the total photoemission (photoelectrons collected over all emission angles) from an identical bound $2s/3s$ wave packet in hydrogen would have a maximal ionization signal at all kinetic energies exactly at the zero relative phase of the wave packet ($\varphi = 0$). Here, we expected a similar effect to occur in ATAS, but figure 3 shows that this is clearly not the case. In order to understand the process of absorption from a bound wave packet in more detail, we must turn to perturbation theory.

4. Perturbation theory

The energy absorbed by the atom can be worked out analytically provided that the test pulse is weak and has a simple shape. If we assume that the complex amplitudes of the bound wave packet are constant,

$$c_j(t) \approx c_j^{(0)}, \tag{20}$$

equal to their initial value before the arrival of the test pulse, then the first-order wave packet generated by the test pulse is

$$|\psi^{(1)}(t)\rangle = \sum\!\!\!\!\!\!\int_f c_f(t) \exp[-i\epsilon_f t]|f\rangle, \tag{21}$$

with complex amplitudes

$$c_f(t) = \frac{1}{i}\sum_j \langle f \mid \hat{p}_z \mid j\rangle c_j \int_{-\infty}^{t} \mathrm{d}t' A(t') \exp[i\omega_{fj} t'], \tag{22}$$

where $\omega_{fj} = \epsilon_f - \epsilon_j$. Given the test pulse in equation (9), the complex amplitudes for the excited wave packet can be written as

$$c_f(t) = \frac{A_0}{2i}\sum_j \langle f \mid \hat{p}_z \mid j\rangle c_j [F_+(t) + F_-(t)], \tag{23}$$

where the time-dependent factors can be evaluated in terms of error functions,

$$F_{\pm}(t) = \mathrm{e}^{\pm i\phi}\int_{-\infty}^{t} \mathrm{d}\tau \exp[i(\omega_{fj} \pm \omega_0)\tau - a\tau^2]$$
$$= -\frac{\mathrm{e}^{\pm i\phi}}{2}\sqrt{\frac{\pi}{a}}\exp\left[-\frac{(\omega_{fj} \pm \omega_0)^2}{4a}\right]$$
$$\times\left[\mathrm{erf}\left(\frac{2at - i(\omega_{fj} \pm \omega_0)}{2\sqrt{a}}\right) + 1\right]. \quad (24)$$

The error function tends to ±one as time goes to ±infinity, which implies that the last factor in equation (24) is zero before the test pulse and two after the test pulse. In general, the $F_{-}(t)$ contribution is larger than the $F_{+}(t)$ contribution because of the resonance condition with the continuum: $\omega_{fj} = \epsilon_f - \epsilon_j \approx \omega_0$. The omission of the $F_{+}(t)$ term is called the rotating wave approximation (RWA).

The time-dependent expectation value of $\hat{p}_z$ is approximated using the zeroth- and first-order wave packet as

$$p_z(t) \approx \langle\psi^{(0)}(t)|\hat{p}_z|\psi^{(1)}(t)\rangle + c.c.$$
$$= \frac{A_0}{2i}\sum_{j',j}\oint\!\!\!\!\!\!-_f\, c_{j'}^{*}c_j\langle j'|\,\hat{p}_z\,|f\rangle\langle f|\,\hat{p}_z\,|j\rangle$$
$$\times \exp[-i\omega_{fj'}t]\{F_{+}(t) + F_{-}(t)\} + c.c., \quad (25)$$

where we can clearly see that the electron makes a transition from any initial wave packet state $j = \{j_1, j_2\}$ to any (dipole-allowed) excited state f and then back to any wave packet state $j' = \{j_1, j_2\}$ with amplitudes proportional to the Fourier transform of the time-factors at the recombination energy, $\omega_{fj'} = \epsilon_f - \epsilon_{j'}$. In the Fourier domain, the expression is indeed simplified to

$$\tilde{p}_z^{\pm}(\omega) = -\frac{A_0}{2\sqrt{2a}}\sum_{j,j'}\oint\!\!\!\!\!\!-_f\, c_{j'}^{*}c_j\langle j'|\,\hat{p}_z\,|f\rangle\langle f\,|\,\hat{p}_z\,|j\rangle$$
$$\times\left\{\frac{\mathrm{p.v.}}{\omega - \omega_{fj'}} - i\pi\delta(\omega - \omega_{fj'})\right\}$$
$$\times\exp\left[\pm i\phi - \frac{(\omega \pm \omega_0 - \omega_{jj'})^2}{4a}\right], \quad (26)$$

where we have obtained a non-resonant principal value term and a resonant delta function term for each separate time factor $F_{\pm}(t)$ in equation (25). We see that the $p_z^{\pm}(\omega)$ expressions for plus and minus are equivalent besides the trivial phase factor of the field and the Gaussian field spectral envelope (the last factor in equation (26)). The p.v. term in equation (26) arises from the time-dependent population of the excited wave packet in equation (24), while the delta term arises from the constant term. The p.v. term was derived by partial integration (boundary terms are neglected) using the fact that the primitive function of the error function is a Gaussian function in time that then transforms to a Gaussian function in energy.

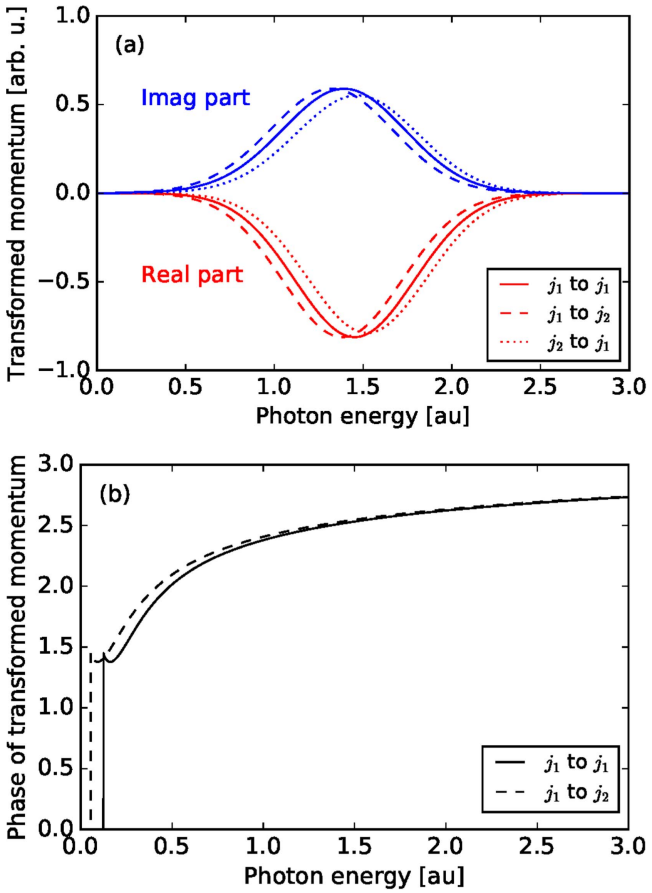

Figure 4. (a) The real and imaginary parts of the transformed momentum. The momentum is separated into an elementary electron scattering process according to equation (28) with elastic processes: $j_1 \to j_1$ and inelastic processes: $j_1 \to j_2$ and $j_2 \to j_1$. The transformed momentum is normalized to the maximal absolute value of all scattering events. (b) The corresponding phase of the transformed separated momentum. All results are computed using the toy model defined in equation (27).

4.1. Toy model: 2s/3s wave packet

The evaluation of equation (26) requires knowledge of the transition matrix elements of the system. Thus, we introduce a simple toy model with transition matrix elements:

$$\langle f\,|\,\hat{p}_z\,|\,j\rangle = \begin{cases}\frac{1}{(1+k)^2}, & \epsilon_f > I_p\\ 0, & \epsilon_f < I_p,\end{cases} \quad (27)$$

where $k = \sqrt{2(\epsilon_f - I_p)}$ is the wave number of the photoelectron. The toy model has two important features: (i) excited bound states are neglected as the transition matrix element is zero for photon energies below the ionization threshold, I_p; and (ii) the transition strength decreases at high photon energies with a characteristic rate of the hydrogen atom. If the termination of the integrand is not enforced, the p.v. integral in equation (26) may diverge. In figure 4(a), we show separate components of the transformed momentum,

$$\tilde{p}_z(\omega) = \sum_{j,j'}\tilde{p}_z(\omega; j', j), \quad (28)$$

corresponding to different electron scattering processes from the initial wave packet state, $|j\rangle$, via all virtual states, $|f\rangle$, to the final wave packet state, $|j'\rangle$. The momentum peaks of the elastic scattering, $j = j'$, are not centered exactly at the central photon energy, $\omega_0 = 1.5$, because of the decreasing transition amplitude with increasing photon energy in the toy model. The transformed momentum of inelastic scattering, $j \neq j'$, is shifted from the elastic case to higher (lower) frequencies when the electron moves to lower (higher) energy wave packet state. The resonant and principal value contributions to the transformed momentum are of comparable magnitude with a phase of $\sim$2.5 radians at the central frequency, as shown in figure 4(b).

Equations (14) and (26) are now combined to find that the absorbed field energy by the atom at $\omega \geqslant 0$ is

$$\frac{\mathrm{d}\Delta E}{\mathrm{d}\omega} \approx -2\omega\,\mathrm{Im}\left\{\sum_{j,j'} \tilde{p}_z^-(\omega; j', j)\tilde{A}^*(\omega)\right\}, \tag{29}$$

where the energy-domain vector potential is

$$\begin{aligned}\tilde{A}(\omega) &= \frac{1}{\sqrt{2\pi}}\int_{-\infty}^{+\infty} \mathrm{d}t' A(t')\exp[i\omega t'] \\ &\approx \mathrm{e}^{\mathrm{i}\phi+\mathrm{i}\omega t_0}\frac{A_0}{2\sqrt{2a}}\exp\left[-\frac{(\omega_0+\omega)^2}{4a}\right],\ \omega < 0.\end{aligned} \tag{30}$$

In writing equation (29), we have also used the RWA, which is well justified for the parameters in equation (8). While $p_z(\omega)$ (equation (26)) has multiple Gaussian field peaks located at $\omega \approx \omega_0 \pm \omega_{jj'}$, energy can only be absorbed when these peaks are within the bandwidth of the test pulse, $\omega \approx \omega_0$, according to equation (29). Clearly, no energy can be absorbed at energies where there is no spectral energy density of the test pulse to begin with.

As already mentioned, an electron in an initial wave packet state $|j\rangle$ can either transition back to the original wave packet state ($j = j'$) so that $\omega_{jj'} = 0$, or it can transition to a different wave packet state ($j \neq j'$) where, in general, $\omega_{jj'} \neq 0$. In this way, it is possible for the atom to absorb the same photon energy from the test pulse by different electron mechanisms, $\tilde{p}_z^-(\omega; j', j)$, with distinct amplitudes and phases, as shown in equation (29). This opens up for interference effects in the absorption of the light, provided that the bandwidth of the test pulse is comparable or larger than the wave packet energy splittings of interest,

$$\Delta\omega_\mathrm{e} = 4\ln(2)/\tau_\mathrm{e} > \omega_{jj'}. \tag{31}$$

We now reintroduce the phase shift between the j_2 and j_1 states, $\varphi = \arg[c_{j_2}/c_{j_1}]$, to study how the absorption process can be controlled by a time delayed test pulse. Clearly, the elastic absorption processes are unaffected by this phase shift since the final wave packet amplitudes is complex conjugated, while the initial is not conjugated, in equation (26). The inelastic scattering terms, however, are affected by the phase shift. The $j_1 \to j_2$ process suffers a phase reduction of $-\varphi$, while $j_2 \to j_1$ gains a phase of $+\varphi$. Taken together, the two inelastic processes lead to a sinusoidal modulation over φ, while the elastic processes give a constant background in the absorption. In this way, the inelastic processes can increase or decrease the absorption of the test pulse depending on the relative phase. The absorption peak of the toy model is shown in figure 5, as a function of photon energy and relative wave packet phase, using false color. The similarities between the exact hydrogen absorption in figure 3 and that of the toy model are striking: the maximal absorption occurs for $\varphi \approx 0$ with a small negative tilt of the peak with increasing photon energy.

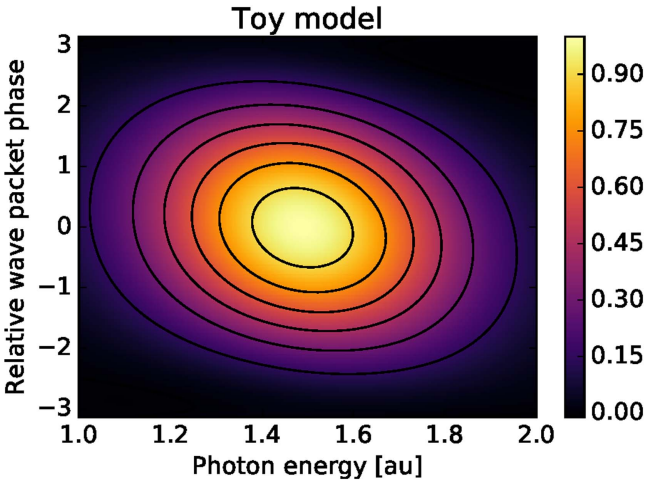

Figure 5. The normalized absorbed energy of the toy model for a two-state wave packet ionized by the test pulse as a function of photon energy, ω, and relative wave packet phase, φ.

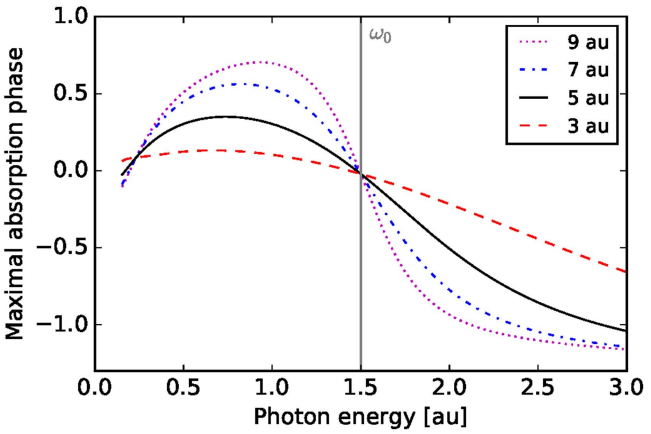

Figure 6. Relative phase that maximizes the absorption in the toy model. The maximal absorption phases associated with different pulse envelope durations, $\tau_e = [3, 5, 7, 9]$, are shown for a fixed central photon energy of $\omega_0 = 1.5$.

In order to make a quantitative analysis of the phase shifts that maximize the absorption, we Fourier transform the data in figure 5 over relative phase, φ, and directly extract the phase of the oscillation. The phase that maximizes absorption is shown in figure 6. It is seen that the phase exhibits a linear region with a negative slope close the the central frequency of the test pulse. For comparison, we also show the maximal absorption phase for shorter test pulses with $\tau_e = 3$ and two longer pulses with $\tau_e = \{7, 9\}$. The negative phase slope is clearly dependent on the pulse duration. It appears that a phase shift of $-\pi/2$ is observed across the peak of the field.

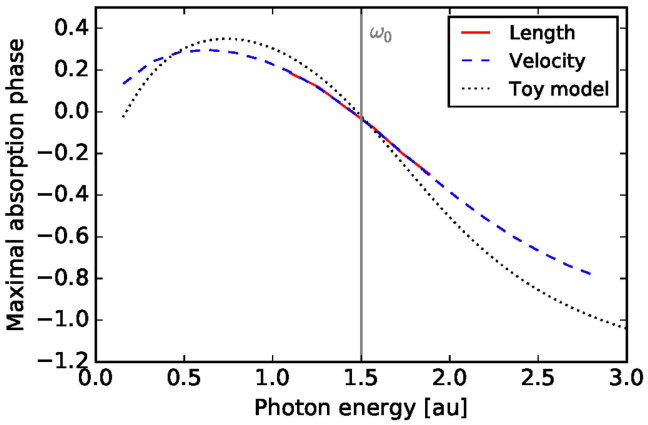

Figure 7. Comparison of the $2s/3s$ wave packet relative phase that maximizes the absorption as a function of photon energy for the exact case hydrogen and the toy model.

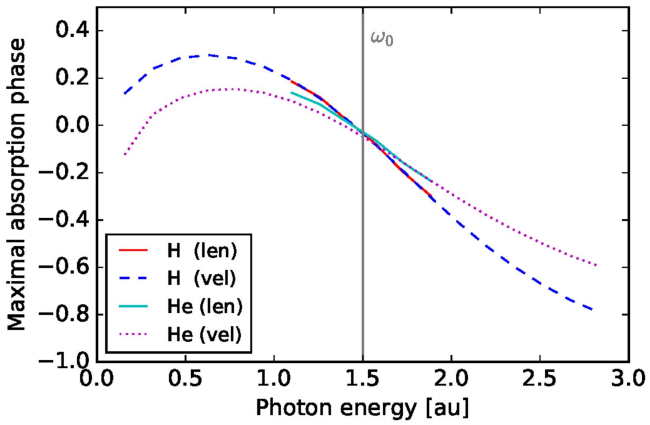

Figure 8. Comparison of the $2s/3s$ wave packet relative phase that maximizes the absorption as a function of photon energy for exact case hydrogen and helium.

Further away from the central frequency, the phase of the toy model exhibits a non-monotonous behavior. The phase flattens out with increasing photon energy. Close to the threshold, however, the phase bends to a positive slope. The exact shape of the phase curve that maximizes absorption depends on the choice of toy model. In the next section, we compare how well our toy model, equation (27), agrees with the exact result in hydrogen, presented in figure 3.

5. Results

We have found that the absorption of a coherent XUV attosecond test pulse by a bound $2s/3s$ wave packet in hydrogen critically depends on the relative phase of the wave packet. The overall absorption is largest when the relative phase of the electron wave packet is close to zero. This is not surprising, because the test pulse allows for constructive photoionization from both initial wave packet states into the continuum. Conversely, a wave packet with a relative π-phase ejects photoelectrons that interfere destructively, thus, making the atom more transparent to the test pulse.

In more detail, we have found that the maximal absorption at different photon energies, within the test pulse, occurs at slightly different relative phases. While the central frequency is absorbed the most at zero relative phase, the general curve undergoes a non-monotonous behavior shown in figure 7. The numerical hydrogen result shows excellent agreement between the length and velocity gauge. The result is also stable against intensity variations, we have obtained the same curves with a test pulse of 100 times as much intensity, i.e. by changing from $A_0 = 0.01$ to $A_0 = 0.1$.

In figure 7, we also show a good qualitative agreement between the hydrogen calculation and the simple toy model presented in section 4.1. The curve is sensitive to the model used to describe the dipole interaction. In this sense, the ATAS technique can be used to probe the time-dependent photoelectron wave packet, equation (22), by inelastic photon scattering back onto the original bound wave packet.

To investigate the generality of our result, we have performed calculations for helium within TDCIS for an initial $1s^{-1}2s/3s$ wave packet. As expected, the absorption is qualitatively the same. One difference is that we do not obtain gauge invariance, but this is a known issue with TDCIS and not specific to our method. The velocity gauge calculation is converged best and we only show the converged length gauge result close to the central frequency in figure 8. Due to the nature of how the helium calculations were made, we can not assign an exact phase between the two initial bound states. We have shifted the relative phase to coincide with the crossing at the central photon energy found in hydrogen.

6. Conclusions

We have found that absorption of an attosecond test pulse can be controlled by the relative phase of a coherent bound wave packet coupled to a resonance-free continuum. To our surprise, we found that the maximal frequency-resolved absorption wave-packet phase varies over the bandwidth of the test pulse. This effect was reproduced with a simple model. ATAS experiments with coherent bound electron wave packets in atoms have already been performed, e.g. by tunnel ionization [3]. We believe that the effect of continuum states should also be present in these experiments, but as a background signal that has so far not been given any attention. The role of this 'background signal' should be more clearly visible if the attosecond pulse bandwidth is centered in a resonance-free region.

Recently, a related phase effect was observed theoretically in photoionization of a bound wave packet by an intense laser pulse, where the phase effect was attributed to time- and intensity-dependent depletion of the initial wave packet states [28]. In our case, however, the phase effect is not due to depletion of the initial wave packet states, but rather due to the time-dependent build-up of the photoelectron wave packet. In this sense, the ATAS method can be used to probe the virtual ionization processes, where a photoelectron is first ejected into the continuum and then (in)elastically scattered

back to the initial bound wave packet. The phase effect occurs already at extremely weak field strengths and it is found to be stable against an increased test pulse intensity. This intrinsic phase lag of the ATAS method is problematic for the accurate characterization of the test pulse because it makes it difficult to disentangle which part of phase contribution comes from the stimulated atomic transitions and which comes from the spectral phases of the test pulse. Since the phase effect in ATAS is quite large, it cannot be assumed to be small compared to the group delay of the attosecond test pulse in general.

Acknowledgments

We thank Andreas Wacker for discussions. JMD is funded by the Swedish Research Council, Grant No. 2014-3724. SP is funded by the the NSF through a grant to ITAMP. EL is funded by the Swedish Research Council, Grant No. 2016-03789.

ORCID iDs

Jan Marcus Dahlström https://orcid.org/0000-0002-5274-1009
Stefan Pabst https://orcid.org/0000-0003-1134-4629
Eva Lindroth https://orcid.org/0000-0003-3444-1317

References

[1] Zewail A H 2000 Femtochemistry: atomic-scale dynamics of the chemical bond *J. Phys. Chem.* A **104** 5660–94
[2] Krausz F and Ivanov M 2009 Attosecond physics *Rev. Mod. Phys.* **81** 163–234
[3] Goulielmakis E *et al* 2010 Real-time observation of valence electron motion *Nature* **466** 739–43
[4] Wirth A *et al* 2011 Synthesized light transients *Science* **334** 195–200
[5] Sabbar M, Timmers H, Chen Y-J, Pymer A K, Loh Z-H, Sayres S G, Pabst S, Santra R and Leone S R 2017 State-resolved attosecond reversible and irreversible dynamics in strong optical fields *Nat. Phys.* **13** 472–8
[6] Pertot Y *et al* 2017 Time-resolved x-ray absorption spectroscopy with a water window high-harmonic source *Science* **355** 264–7
[7] Wang H, Chini M, Chen S, Zhang C H, He F, Cheng Y, Wu Y, Thumm U and Chang Z 2010 Attosecond time-resolved autoionization of argon *Phys. Rev. Lett.* **105** 143002
[8] Ott C, Kaldun A, Raith P, Meyer K, Laux M, Evers J, Keitel C H, Greene C H and Pfeifer T 2013 Lorentz meets Fano in spectral line shapes: a universal phase and its laser control *Science* **340** 716–20
[9] Ott C *et al* 2014 Reconstruction and control of a time-dependent two-electron wave packet *Nature* **516** 374–8
[10] Anand M, Pabst S, Kwon O and Kim D E 2017 Attosecond counter-rotating-wave effect in xenon driven by strong fields *Phys. Rev.* A **95** 53420
[11] Beck A R, Neumark D M and Leone S R 2015 Probing ultrafast dynamics with attosecond transient absorption *Chem. Phys. Lett.* **624** 119–30
[12] Chu W C and Lin C D 2013 Absorption and emission of single attosecond light pulses in an autoionizing gaseous medium dressed by a time-delayed control field *Phys. Rev.* A **87** 013415
[13] Pabst S, Sytcheva A, Moulet A, Wirth A, Goulielmakis E and Santra R 2012 Theory of attosecond transient-absorption spectroscopy of krypton for overlapping pump and probe pulses *Phys. Rev.* A **86** 063411
[14] Wu M, Chen S, Camp S, Schafer K J and Gaarde M B 2016 Theory of strong-field attosecond transient absorption *J. Phys. B: At. Mol. Opt. Phys.* **49** 62003
[15] Pabst S and Dahlström J M 2016 Eliminating the dipole phase in attosecond pulse characterization using Rydberg wave packets *Phys. Rev.* A **94** 13411
[16] Pabst S and Dahlström J M 2017 Characterizing attosecond pulses in the soft x-ray regime *J. Phys. B: At. Mol. Opt. Phys.* **50** 104002
[17] Scrinzi A 2010 Infinite-range exterior complex scaling as a perfect absorber in time-dependent problems *Phys. Rev.* A **81** 53845
[18] de Boor C 1980 A practical guide to splines *Math. Comput.* **34** 325
[19] Lindgren I and Morrison J 1986 Atomic Many-Body Theory *Series on Atoms and Plasmas* 2nd edn (New York: Springer)
[20] Mårtensson A-M and Salomonson S 1982 Specific mass shifts in Li and K calculated using many-body perturbation theory *J. Phys. B: At. Mol. Opt. Phys.* **15** 2115–30
[21] Dahlström J M, Carette T and Lindroth E 2012 Diagrammatic approach to attosecond delays in photoionization *Phys. Rev.* A **86** 61402
[22] Dahlström J M and Lindroth E 2014 Study of attosecond delays using perturbation diagrams and exterior complex scaling *J. Phys. B: At. Mol. Opt. Phys.* **47** 124012
[23] Simon B 1979 The definition of molecular resonance curves by the method of exterior complex scaling *Phys. Lett.* A **71** 211–4
[24] Scrinzi A 2010 Infinite-range exterior complex scaling as a perfect absorber in time-dependent problems *Phys. Rev.* A **81** 053845
[25] Greenman L, Ho P J, Pabst S, Kamarchik E, Mazziotti D A and Santra R 2010 Implementation of the time-dependent configuration-interaction singles method for atomic strong-field processes *Phys. Rev.* A **82** 023406
[26] McCurdy C W, Stroud C K and Wisinski M K 1991 Solving the time-dependent Schrödinger equation using complex-coordinate contours *Phys. Rev.* A **43** 5980–90
[27] Sakurai J J 1985 *Modern Quantum Mechanics* (Reading, MA: Addison-Wesley) (https://doi.org/10.1119/1.14491)
[28] Pazourek R, Reduzzi M, Carpeggiani P A, Sansone G, Gaarde M and Schafer K 2016 Ionization delays in few-cycle-pulse multiphoton quantum-beat spectroscopy in helium *Phys. Rev.* A **93** 023420